

Multi-wavelength Observations of Sgr A* – I. 18 July 2019

JOSEPH M. MICHAIL ¹, MARK WARDLE ², FARHAD YUSEF-ZADEH¹, AND DEVAKY KUNNERIATH ³

¹Center for Interdisciplinary Exploration and Research in Astrophysics (CIERA) and Department of Physics and Astronomy, Northwestern University, 1800 Sherman Ave., Evanston, IL 60201, USA

²Research Centre for Astronomy, Astrophysics and Astrophotonics and Department of Physics and Astronomy, Macquarie University, Sydney, NSW 2109, Australia

³National Radio Astronomy Observatory, 520 Edgemont Road, Charlottesville, VA 22903, USA

Submitted to ApJ

ABSTRACT

We present and analyze ALMA submillimeter observations from a multi-wavelength campaign of Sgr A* during 18 July 2019. In addition to the submillimeter, we utilize concurrent mid-IR (*Spitzer*) and X-ray (*Chandra*) observations. The submillimeter emission lags $\delta t = 21.48_{-3.57}^{+3.44}$ minutes behind the mid-IR data. The entire submillimeter flare was not observed, raising the possibility that the time delay is a consequence of incomplete sampling of the light curve. The decay of the submillimeter emission is not consistent with synchrotron cooling. Therefore, we analyze these data adopting an adiabatically expanding synchrotron source that is initially optically thick or thin in the submillimeter, yielding time-delayed or synchronous flaring with the IR, respectively. The time-delayed model is consistent with a plasma blob of radius $0.8 R_S$ (Schwarzschild radius), electron power-law index $p = 3.5$ ($N(E) \propto E^{-p}$), equipartition magnetic field of $B_{\text{eq}} \approx 90$ Gauss, and expansion velocity $v_{\text{exp}} \approx 0.004c$. The simultaneous emission is fit by a plasma blob of radius $2 R_S$, $p = 2.5$, $B_{\text{eq}} \approx 27$ Gauss, and $v_{\text{exp}} \approx 0.014c$. Since the submillimeter time delay is not completely unambiguous, we cannot definitely conclude which model better represents the data. This observation presents the best evidence for a unified flaring mechanism between submillimeter and X-ray wavelengths and places significant constraints on the source size and magnetic field strength. We show that concurrent observations at lower frequencies would be able to determine if the flaring emission is initially optically thick or thin in the submillimeter.

Keywords: Galactic center (565), Active galactic nuclei (16), Supermassive black holes (1663)

1. INTRODUCTION

Sagittarius A* (Sgr A*) is the $4.297 \times 10^6 M_{\odot}$ supermassive black hole located at a distance of 8.27 kpc (Gravity Collaboration et al. 2019) in the center of the Milky Way Galaxy. It is known to be a variable source at radio through X-ray wavelengths (e.g., Yusef-Zadeh et al. 2006; Dodds-Eden et al. 2009; Dexter et al. 2014; Hora et al. 2014) and is a prime target to understand how gas is captured, accreted, and/or ejected from low-luminosity supermassive black holes.

At infrared (IR) and X-ray wavelengths, the emission from Sgr A* is optically thin synchrotron radiation (Eckart et al. 2004, 2006). At submillimeter (submm) and radio wavelengths, the variable emission's timescale is much shorter than that of the synchrotron cooling time. Yusef-Zadeh et al. (2006) used an adiabatically expanding synchrotron plasma (van der Laan 1966) to describe the emission observed in this frequency range with much success. Since then, there has been a formidable effort to connect the radio/submm and IR/X-ray regimes with a model that can explain the variable emission across the electromagnetic spectrum. Multi-wavelength campaigns (e.g., Yusef-Zadeh et al. 2008; Eckart et al. 2009; Mossoux et al. 2016) are critical to test this picture. Non-overlapping observations

(due to the rise/set times at different observatories) and time-delayed emission at radio frequencies make this a difficult task. This has been somewhat alleviated by space-based IR instruments, like the Spitzer Space Telescope, in concert with submm observations, like ALMA (Witzel et al. 2018). Submm observations are key as they lay near the “submillimeter bump,” (Zylka et al. 1992, 1995) where Sgr A* is brightest. This bump begins in the millimeter (mm) and decays at wavelengths near the far-IR, where the emission becomes increasingly optically thin, and optical depth effects are unimportant (Marrone 2006).

Abuter et al. (2021) recently published an analysis from a multi-wavelength campaign on 18 July 2019 using IR and X-ray data. Here, we present simultaneous ALMA observations, which show a time delay relative to the mid-IR data, suggesting an optically thick and dynamically evolving source.

2. OBSERVATIONS AND DATA REDUCTION

The campaign included data from the VLA and GMRT on 18 July 2019; however, these light curves are not useful for this date. The VLA data at Q-band could not be calibrated by the VLA pipeline owing to bad weather and long cycle times. Extended structures in the GMRT data dominated Sgr A*, and identifying the intrinsic variability of Sgr A* is difficult. A more detailed accounts of these data will be given in Michail et al. (2021d, in prep.).

2.1. Submillimeter: ALMA

The ALMA data used were taken as part of a Cycle 6 ACA observatory filler program (project code 2018.A.00050.T), which observed the Galactic Center in Band 7 on 18 July 2019 for about 7 hours. The dataset was calibrated and imaged by the ALMA pipeline (Pipeline-CASA54-P1-B, r42254, CASA v5.4.0-70, McMullin et al. 2007). The calibrated measurement set was obtained by restoring the calibration from the ALMA archive using `scriptForPI.py`. The data consist of 4 spectral windows of 2 GHz bandwidth and a spectral resolution of 1.953 MHz, with one spectral window centered on the CO transition at 346 GHz and three continuum spectral windows. J1337-1257 and J1924-2914 were used as bandpass and amplitude calibrators. J1700-2610 (J1700) and J1717-3342 were used as phase calibrators throughout the observation. J1733-3722 (J1733) was the phase calibrator during the final execution block. There was an offset in the fluxes ($\approx 10\%$) between the first three executions, which used the same phase calibrator. To correct this offset, we scaled the fluxes of the second and third execution blocks to match the first execution block. The observation was imported into AIPS

for phase self-calibration. Then, DFTPL was used to extract the light curves from Sgr A* at a 60 second binning time. The light curve for each spectral window is calculated independently using baselines greater than 20 k λ . The ALMA light curves are shown in Figure 1 (left).

2.2. Mid-infrared: Spitzer

We obtained the binned *Spitzer* light curves of Sgr A* for this day of observation (*Spitzer* Sgr A* Collaboration, priv. comm.), which were originally published in Abuter et al. (2021). Details of these observations are given in the aforementioned paper. Briefly, the IRAC instrument (Fazio et al. 2004) on the Spitzer Space Telescope (Werner et al. 2004) observed Sgr A* as part of *Spitzer* program 14026 (Fazio et al. 2018) at 4.5 μm . The total on-source time for this observation was approximately 16 hours. Hora et al. (2014) and Witzel et al. (2018) give further details on the observing mode and data reduction. Fluxes shown are relative to a period where Sgr A* is semi-quiet and are not absolute (Hora et al. 2014). These data are de-reddened using the extinction value in Fritz et al. (2011) for the Band 2 IRAC instrument ($A_{4.5 \mu\text{m}} = 1.06$ mag). This yields a correction factor $f_{4.5 \mu\text{m}} = 2.512^{1.06} = 2.65$. The de-reddened *Spitzer* light curve for 18 July 2019 is shown in Figure 1 (center).

2.3. X-ray: Chandra

Three days of simultaneous observations of Sgr A* were completed with the Chandra X-Ray Observatory. The corresponding observation ID for 18 July 2019 is 22230 (PI: Fazio) and was first published in Abuter et al. (2021). This observation lasted 52 ks using *Chandra*’s FAINT mode. Sgr A* was centered on the ACIS-S3 chip using the 1/8 subarray mode to reduce the possibility of pileup events from bright Galactic Center sources. The data are reprocessed with CHANDRA_REPRO using CIAO v4.13 and CALDB v4.9.4. The WCS solutions are corrected using the `wcs_match` and `wcs_update` scripts utilizing 3 X-ray bright sources near Sgr A* from the Chandra Source Catalogue (Evans et al. 2010, CSC) in DS9. One of these three sources is the nearby magnetar (SGR J1745-2900) that was readily apparent. The norm of the WCS correction is about 2 pixels (1”). Finally, the `axbary` script is used to apply barycentric time corrections to the time stream data.

To obtain background-subtracted light curves of Sgr A*, we follow Capellupo et al. (2017, and references therein). A 1”25 radius aperture is centered at the J2000.0 radio location of Sgr A* (17^h45^m40^s.04, -29°00’28”18) to minimize contamination from the nearby magnetar. We only extract

events within the 2 – 8 keV range to minimize photons from the diffuse X-ray background (e.g., Neilsen et al. 2013). An aperture of radius 10'' is centered on 17^h45^m40^s.30, –28°59'52".66 as the background region. The CSC is used to check for known sources within this area. No obvious point or extended sources are in this region which would bias our results. A 300 second binning time is adopted following previous light curve analyses of this source.

To detect flaring emission, we use an open-source Bayesian blocks Python module called `bblocks`¹ (Scargle 1998; Scargle et al. 2013; Williams et al. 2017) with a false positive rate of $p_0 = 0.05$. The light curves of Sgr A* and the Bayesian block results are shown in Figure 1 (right).

3. RESULTS

The ALMA, *Spitzer*, and *Chandra* light curves for these observations all show the presence of flaring emission. Unfortunately, the submm flare peak appears to occur between ALMA execution blocks. However, a sufficient amount of the flare is present to complete cross-correlations with the other simultaneous observations. Throughout this paper, we use the `pyCCF` (Peterson et al. 1998; Sun et al. 2018) Python module with 5000 Monte Carlo simulations to check for possible delays in the peak emission. A histogram of the 5000 centroid lag times is made, and we characterize the spread in the time delay using the 95% (2σ) confidence interval (CI). We consider a statistically significant time lag if 0 is not contained within this interval. The mean and 95% CI error range is denoted on each histogram plot.

We check for a time delay between the most widely separated ALMA frequencies; the histogram is shown in Figure 2 (left). We do not find evidence of a time delay between the ALMA frequencies. However, we find a statistically significant time delay of $\delta t = 21.48_{-3.57}^{+3.44}$ minutes between the 334 GHz and mid-IR light curves, where the submm emission is lagging (Figure 2, center). As a secondary check, we use the ZDCF cross correlation code (Alexander 1997) along with the PLIKE program (Alexander 2013) on the submm and mid-IR light curves. We find a time delay of $\delta t = 22.00_{-6.77}^{+5.86}$ minutes, consistent with the value from `pyCCF`. A close-up plot of these two light curves is shown in Figure 3 (left). Eckart et al. (2008) detected delayed flaring emission at 345 GHz relative to near-IR data on the order of 1.5 ± 0.5 hours. Eckart et al. (2009) lists modeled time

delays between the IR to submm/radio bands, which range from 0.3 to 1.7 hours. Fazio et al. (2018) detected an approximate 20 minute time delay between *Spitzer* and SMA observations at 345 GHz. The time delay we calculate between the *Spitzer* and ALMA data here is well-matched with those previously published in the literature.

We find that the 2-8 keV flare is simultaneous with the mid-IR data using `pyCCF` (Figure 2, right) and agrees with the ZDCF analysis that we perform ($\delta t = 2.25_{-4.39}^{+8.72}$ minutes). These results are consistent with the previous analysis of this data (Abuter et al. 2021, Boyce et al., in preparation). Additionally, the observed flaring emission in the K- (2.2 μm) and H-filters (1.63 μm) are simultaneous with the *Spitzer* observations (Abuter et al. 2021). The lack of time delay at these higher frequencies matches expectations from the adiabatically expanding picture, where the IR data are optically thin.

Due to non-continuous ALMA execution blocks, the true submm flare peak may not have been observed. We use a Bayesian analysis technique known as Gaussian Process (GP) Regression from the `sklearn` Python package (Pedregosa et al. 2011) to interpolate the missing data. Our kernel is a compound radial-basis + constant function, which we use to fit the lowest frequency ALMA data. In the lower-left panel of Figure 3 (right), we show the observed ALMA data (red) and the mean GP fit (black). The shaded purple region is the 95% CI of the fit. We complete a cross-correlation between ALMA and *Spitzer* using `pyCCF` using the GP fitted data and their 68% (1σ) CI errors to be consistent with the analysis above. The cross-correlation histogram is shown in the right panel, where we find $\delta t = 15.39_{-1.62}^{+1.62}$ minutes. This is similar to the time delay value found using `pyCCF` and ZDCF.

Both methods find time delayed emission between the peaks of the submm and mid-IR data. The three test models presented by Abuter et al. (2021) are not able to produce time delayed emission, which is indicative of an optically thick and dynamically evolving source, nor can it match the observed peak 334 GHz flux. Both point toward submm emission production via an optically thick adiabatically-expanding plasma (van der Laan 1966; Yusef-Zadeh et al. 2006). We consider this possibility in Section 4.

4. ANALYSIS

In Section 3, we applied two different methods to check the statistical significance of the observed time delay between the submm and mid-IR light curves. However, the gap in our submm data near the peak allows for a range of possible conditions, namely, both simultaneous

¹ The open-source Bayesian Blocks algorithm produced by Peter Williams is located here: <https://pwkit.readthedocs.io/en/latest/science/pwkit-bblocks/>.

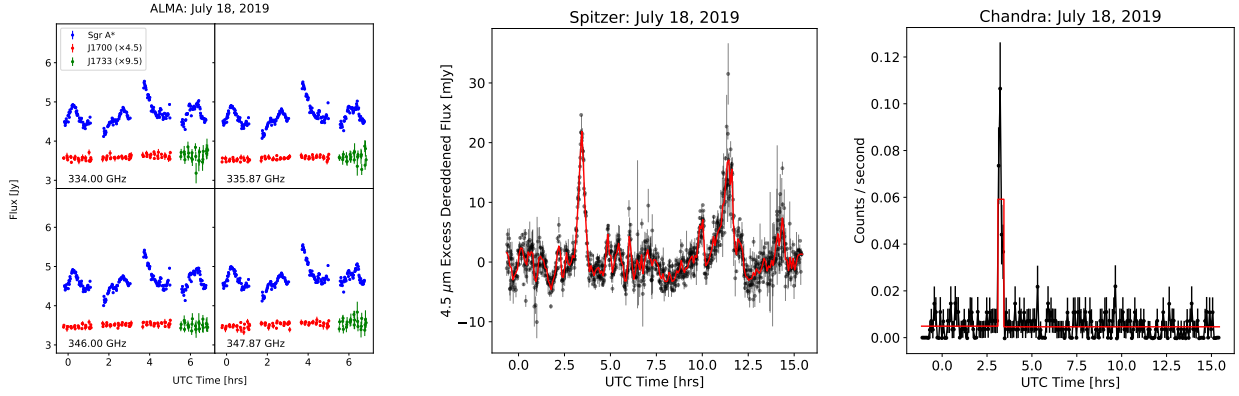


Figure 1. Multi-wavelength light curves of Sgr A* on 18 July 2019. *Left:* Sgr A* (blue) as observed by ALMA; the phase calibrators J1700 and J1733 (red and green, respectively) are shown. A 60-second binning time is used. *Center:* De-reddened *Spitzer* light curve of Sgr A* at 60-second binning (black) and 5-minute binning (red). *Right:* *Chandra* 2-8 keV background-subtracted light curve of Sgr A* at 5-minute binning (black). The Bayesian Block results are plotted in red.

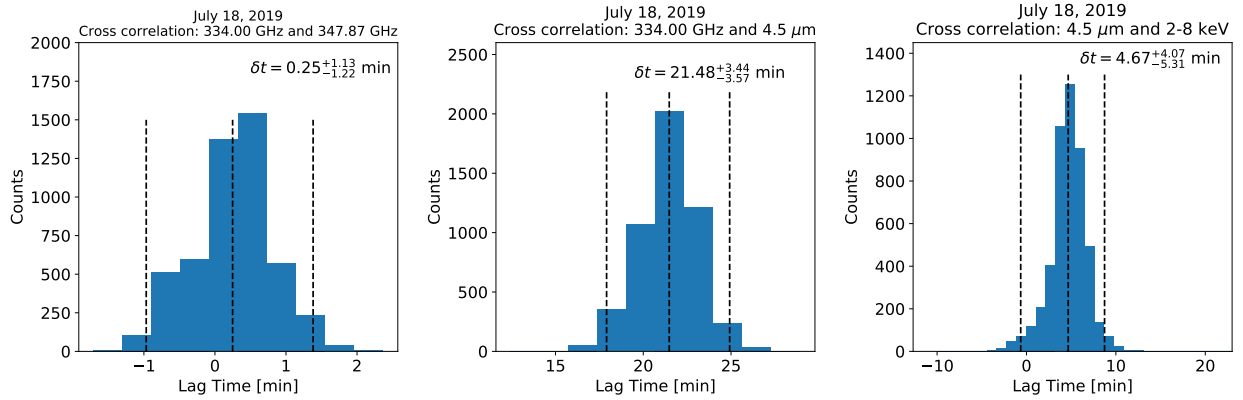


Figure 2. The centroid histograms of cross correlations between pairs of light curves using the `pyCCF` Python package (Sun et al. 2018). The 95% (2σ) confidence interval (CI) is shown denoted. *Left:* The cross correlations between most widely separated ALMA frequencies. *Center:* The cross correlation histogram between the lowest ALMA frequency and *Spitzer* light curves; the ALMA light curve peaks approximately 21 minutes after the *Spitzer* data. *Right:* The cross correlation histogram between *Spitzer* and *Chandra*, where the flaring peaks simultaneously occur.

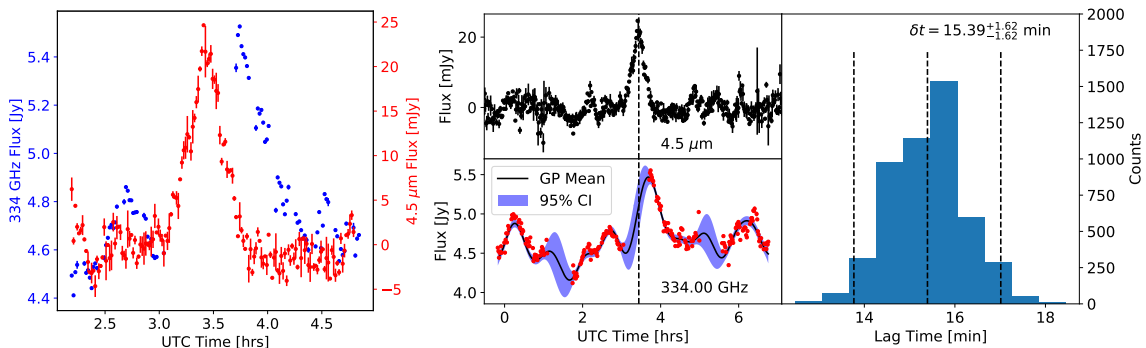


Figure 3. *Left:* Close-up plot of ALMA (blue) and *Spitzer* (red) flaring emission detected on this night of observation. *Right:* The cross-correlation analysis between the *Spitzer* data and Gaussian Process (GP) regressed ALMA light curve. In the bottom left panel, the solid black line represents the mean GP light curve, and the shaded purple region is the 95% CI for the regressed data. The right panel shows the cross-correlation histogram between the two light curves.

and time-delayed emission relative to the mid-IR data. If the submm emission is time delayed, the total peak flux is approximately 5.5 Jy (requiring a peak flare flux ≈ 0.9 Jy). If the emission is simultaneous, the total flux is ≈ 6 Jy with a peak flare flux of ≈ 1.4 Jy. This latter value is estimated using a linear extrapolation of the submm data between $t=3:36:00-4:12:00$ hrs UTC. Note that peak flare fluxes for the simultaneous and time-delayed cases were calculated assuming a quiescent flux of ≈ 4.6 Jy, approximated from the ALMA light curve.

4.1. Can the Gravity model reproduce the submm emission?

We focus on the parameters of the synchrotron model $\text{PLCool}\gamma_{max}$ (PLC) as described by [Abuter et al. \(2021\)](#), which they note is their best-fitting model. With no knowledge of the submm emission, a synchrotron-powered flare (with a cooling break and high-energy cut-off) can describe the IR and X-ray data. However, our analysis above shows a statistically significant time delay between the mid-IR and submm bands. In this case, a pure synchrotron model is insufficient to describe the submm emission.

The flare detected using *Spitzer* at $4.5 \mu\text{m}$ had a reddened-corrected flux of approximately 20 mJy. The corresponding Gravity K- and H-filter data is consistent with an electron power-law index of $p = 2$ ($N(E) \propto E^{-p}$) and implies an IR spectrum of $S_\nu \propto \nu^{-0.5}$. The other two parameters in their model are the radius of the flaring region and magnetic field strength, for which they choose $1 R_S$ (Schwarzschild radius) and 30 Gauss, respectively. For $M_{\text{BH}} = 4.297 \times 10^6 M_\odot$, $1 R_S = 1.27 \times 10^{12}$ cm.

We use these parameters in the context of the adiabatic expansion picture to determine the submm emission. For a spherical region emitting synchrotron radiation, the observed flux (S_0), radius (R_0), and optical depth (τ_0) at frequency ν_0 are related by:

$$S_0 = \frac{\pi R_0^2}{d^2} J_0 (1 - e^{-\tau_0}). \quad (1)$$

d is the distance to the Galactic Center, and J_0 is the source function of a power-law synchrotron source, which is a function of p , ν_0 , and B . Solving for the mid-IR optical depth yields $\tau_{\text{IR}} = 1.36 \times 10^{-8}$. In the adiabatic picture, p and the critical optical depth (where the plasma blob becomes optically thin), τ_{crit} , are related via:

$$e^{\tau_{\text{crit}}} - \left(\frac{2p}{3} + 1\right) \tau_{\text{crit}} - 1 = 0, \quad (2)$$

([Yusef-Zadeh et al. 2006](#)). The flux and opacity at any radius R and frequency ν are determined by

$$S_\nu(R) = S_0 \left(\frac{\nu}{\nu_0}\right)^{5/2} \left(\frac{R}{R_0}\right)^3 \frac{1 - e^{-\tau_\nu}}{1 - e^{-\tau_0}}, \quad (3)$$

and

$$\tau_\nu(R) = \tau_0 \left(\frac{\nu}{\nu_0}\right)^{-(0.5p+2)} \left(\frac{R}{R_0}\right)^{-(2p+3)}. \quad (4)$$

With $\tau_{\text{IR}} = 1.36 \times 10^{-8}$, $\nu_0 = 66.6$ THz ($c/\nu_0 = 4.5 \mu\text{m}$), $p = 2$, $R = R_S$, and a critical optical depth of $\tau_{\text{crit}} = 1.51$, the submm opacity at 334 GHz is $\tau_{\text{submm}} = 0.11$. Since $\tau_{\text{submm}} < \tau_{\text{crit}}$, the submm emission is optically thin and expansion cannot produce a time-delayed submm flare, these parameters produce a submm peak that is simultaneous with the mid-IR. At 334 GHz, the peak flare flux is 0.27 Jy, which underestimates the submm peak flux by a factor of ≈ 2 . Therefore, we consider models with steeper spectra ($p > 2$), and use the adiabatic expansion model to calculate physical parameters consistent with the submm and IR data in both cases of simultaneous and time-delayed emission.

4.2. Case 1: Optically Thin Submm Emission

The choice of p will affect if the submm emission is delayed relative to the mid-IR. Additionally, it will influence physical parameters such as the equipartition magnetic field strength, cooling time, and initial radius. We show how these parameters depend on p in Figure 4 (left). In these illustrative calculations, we assume the peak flare fluxes at 334 GHz and $4.5 \mu\text{m}$ are 1 Jy and 20 mJy, respectively. When calculating the equipartition magnetic field strength, B_{eq} , we assume the electron power-law index is valid between energies of 10 MeV to 1 GeV ($20 \leq \gamma_e \leq 2000$), and neglect the presence of protons or thermal electrons.

In the optically thin case, the flare submm-to-IR spectrum is consistent with $S_\nu \propto \nu^{-0.75}$ (using the peak flare fluxes at $4.5 \mu\text{m}$ and 334 GHz noted above). Such an optically thin spectrum is produced when $p = 2.5$. For this value for p , the equipartition magnetic field strength is $B_{\text{eq}} \approx 27$ Gauss with an initial radius of $R \approx 2 R_S$. These parameters predict K- and H-filter peak fluxes of ≈ 12 mJy and ≈ 9 mJy, respectively (Figure 4, right). The K-filter flux is close to the observed value, but the H-filter flux is underestimated. This is possibly due to a systematic error in the marginal H-filter uncertainty estimate ([Abuter et al. 2021](#)). However, the spectrum may flatten between the submm and IR as it does between the IR and X-ray ([Abuter et al. 2021](#)).

The synchrotron cooling time for the electrons dominating the submm emission exceeds 2 hours, much

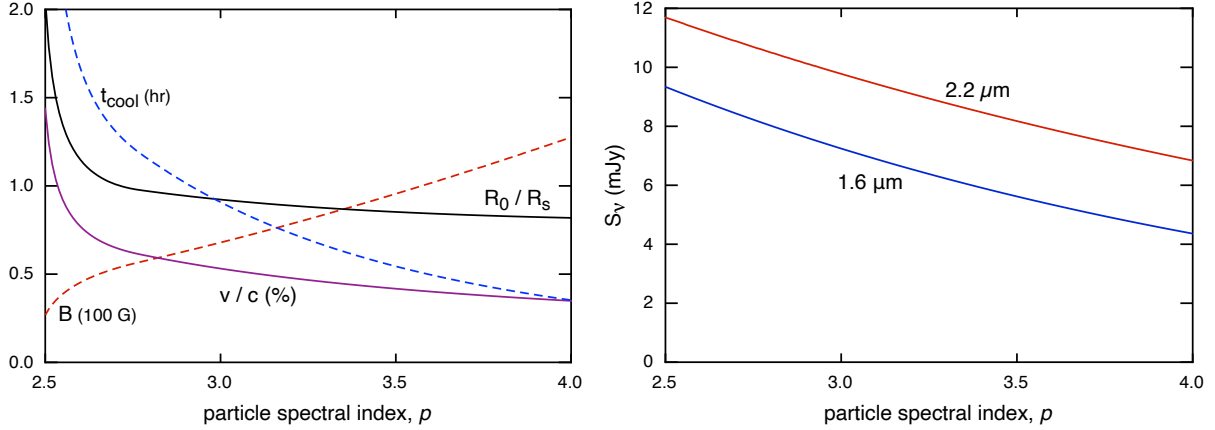


Figure 4. Predicted parameters of the flaring region assuming peak 334 GHz and 4.5 μm fluxes of 1 Jy and 20 mJy, respectively. *Left:* Physical parameters of the adiabatic expansion model as a function of p . The synchrotron cooling time (blue), initial radius (in terms of R_S , black), equipartition magnetic field strength (red), and expansion velocity (purple) are plotted. *Right:* The predicted peak fluxes for the K- (2.2 μm) and H- (1.63 μm) filters as a function of p .

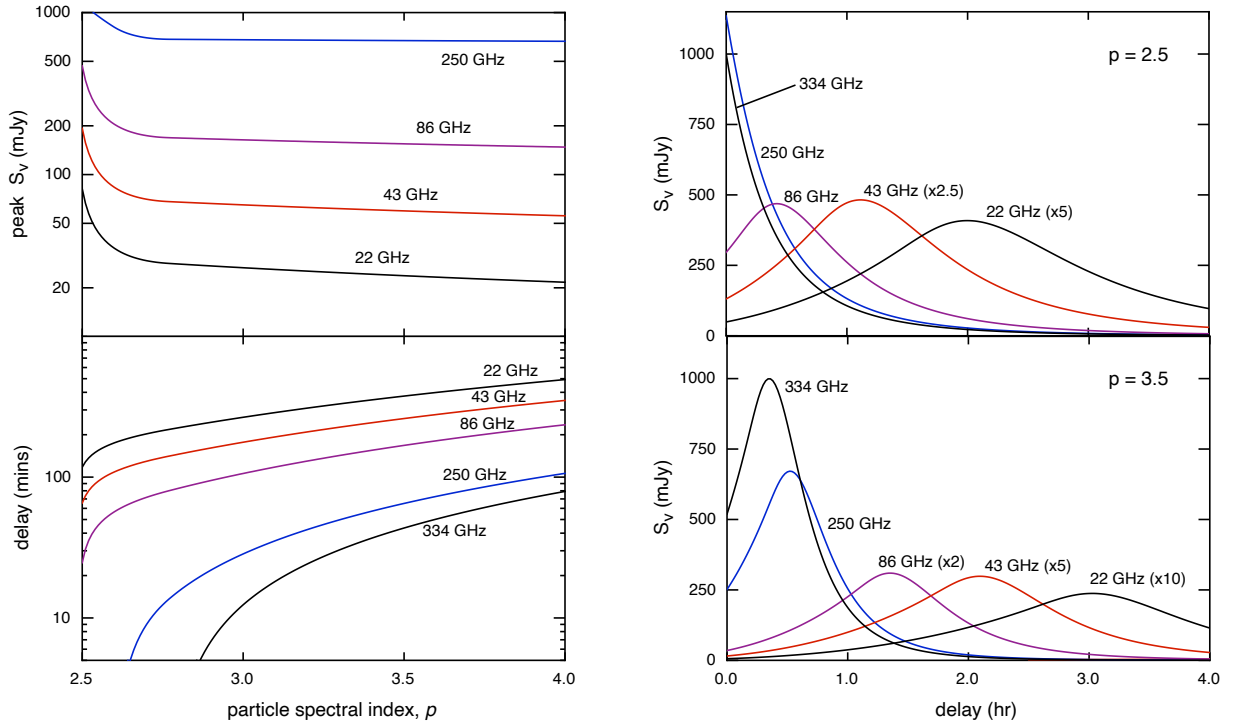


Figure 5. *Left:* Predicted peak fluxes (top) at four representative radio, mm, and submm wavelengths. Predicted time delays (bottom) relative to the 4.5 μm emission as a function of p . *Right:* Light curves for the 4 representative frequencies and the observed submm data observed here for $p = 2.5$ (top) and $p = 3.5$ (bottom).

longer than the observed flare lifetime, suggesting that the submm decay is either due to the escape of synchrotron-emitting electrons from the source region or by adiabatic cooling as the region expands. We focus on the latter scenario here as it leads to testable predictions; the former possibility is poorly constrained. A factor of 2 decline in the flare flux occurs over approximately 15 minutes (estimated from Figure 3, left). With $S_\nu(t) \propto$

$R^{-2p} = R^{-5}$ in the optically thin case, we estimate an expansion velocity $v_{\text{exp}} = (2^{1/5} - 1)R_0/(900 \text{ seconds}) = 0.014c$ at lower frequencies, within the typical range $v_{\text{exp}} = 0.003c - 0.1c$ inferred for previous flares at radio/mm frequencies (Yusef-Zadeh et al. 2008). This model cannot explain the 20 minute time delay between submm and IR wavelengths, but radio/mm observations would be delayed (Figure 5, top right panel).

4.3. Case 2: Time-Delayed Submm Emission

For $p \geq 2.8$, τ_{submm} at the time of the $4.5 \mu\text{m}$ peak is high enough to delay the submm peak due to the transition from an optically thick to thin plasma as the synchrotron source expands. For values of p that are just above 2.8, the expansion speed is too slow to match the 20 minute lag of the 334 GHz light curve relative to the IR (lower left panel of Figure 5). A steeper electron spectrum with $p \approx 3.5$ is preferred to match both the 20 minute time delay and the 15 minute decay timescale. Then, $R \approx 0.8R_S$, $B_{\text{eq}} \approx 90$ Gauss, and $v_{\text{exp}} \approx 0.004c$. The light curves for the representative radio/mm/submm frequencies are shown in Figure 5 (bottom right).

Simultaneous, multi-wavelength observations of Sgr A* at all accessible frequencies should not be undervalued. Figure 5 shows that the ambiguity of the models for the submm-IR time delay can be broken by observing at least one lower frequency.

5. SUMMARY AND CONCLUSIONS

We have reported and analyzed the submm light curve of Sgr A* observed as part of a global multi-wavelength campaign on 18 July 2019. We confirm that the mid-IR data, observed with the Spitzer Space Telescope, is simultaneous with soft X-ray emission detected with the Chandra X-ray Observatory. Our analysis finds a statistically significant time delay between the submm light curve, taken with ALMA, and the *Spitzer* mid-IR light curve. However, the submm data do not sample the entire flare. We analyze the submm and mid-IR emission using adiabatically expanding synchrotron plasma models. We prefer an electron energy spectrum with $p = 2.5$ if the submm emission is initially optically thin. We do not make conclusions about the electron spectrum at high energies, as a cooling break and high energy cut-off is preferred (Abuter et al. 2021) but is not modeled here. Since the submm and mid-IR time delay is not certain, we calculate physical parameters of the flaring emission for different values of the electron power-law index, p , which cover both optically thick and thin models. If the submm-to-IR time delay is truly absent, an adiabatically-expanding plasma with $p = 2.5$, $R \approx 2 R_S$, equipartition magnetic field strength of $B_{\text{eq}} \approx 27$ Gauss, and expansion speed $v_{\text{exp}} \approx 0.014c$ can model the data. If the submm emission is delayed relative to the mid-IR, an adiabatically-expanding plasma

with initial radius $R \approx 0.8R_S$, $p = 3.5$, $B_{\text{eq}} \approx 90$ Gauss, and $v_{\text{exp}} \approx 0.004c$ is preferred. In either case, the need for an expanding source region is clear. We showed that multi-wavelength observations using at least one lower frequency band would have been able to break the degeneracy and should be part of future multi-wavelength campaigns.

1 The authors are greatly appreciative to the *Spitzer* Sgr
 2 A* Collaboration for allowing us to use their data in
 3 this analysis. This work is partially supported by the
 4 grant AST-0807400 from the the National Science Founda-
 5 tion. This paper makes use of the following ALMA
 6 data: ADS/JAO.ALMA#2018.A.00050.T. ALMA is a
 7 partnership of ESO (representing its member states),
 8 NSF (USA) and NINS (Japan), together with NRC
 9 (Canada), MOST and ASIAA (Taiwan), and KASI (Re-
 10 public of Korea), in cooperation with the Republic of
 11 Chile. The Joint ALMA Observatory is operated by
 12 ESO, AUI/NRAO and NAOJ. This work is based on
 13 archival data obtained with the Spitzer Space Telescope,
 14 which was operated by the Jet Propulsion Laboratory,
 15 California Institute of Technology under a contract with
 16 NASA. The scientific results reported in this article are
 17 based in part on data obtained from the Chandra Data
 18 Archive. This research has made use of software pro-
 19 vided by the Chandra X-ray Center (CXC) in the ap-
 20 plication packages CIAO. This research has made use of
 21 data obtained from the Chandra Source Catalog, pro-
 22 vided by the Chandra X-ray Center (CXC) as part of
 23 the Chandra Data Archive. This research was supported
 24 in part through the computational resources and staff
 25 contributions provided for the Quest high performance
 26 computing facility at Northwestern University which is
 27 jointly supported by the Office of the Provost, the Office
 28 for Research, and Northwestern University Information
 29 Technology.

Software: CASA (McMullin et al. 2007), CIAO, bblocks (Scargle 1998; Scargle et al. 2013; Williams et al. 2017), pyCCF (Peterson et al. 1998; Sun et al. 2018), ZDCF (Alexander 1997), PLIKE (Alexander 2013), sklearn (Pedregosa et al. 2011), Scipy (Virtanen et al. 2020), Jupyter Notebook (Kluyver et al. 2016), Pandas (McKinney et al. 2010), Matplotlib (Hunter 2007)

Facilities: ALMA, Spitzer (IRAC), Chandra (ACIS)

REFERENCES

- Abuter, R., Amorim, A., Bauböck, M., et al. 2021, arXiv e-prints, arXiv:2107.01096.
<https://arxiv.org/abs/2107.01096>
- Alexander, T. 1997, Is AGN Variability Correlated with Other AGN Properties? ZDCF Analysis of Small Samples of Sparse Light Curves, Vol. 218, 163, doi: 10.1007/978-94-015-8941-3_14

- . 2013, arXiv e-prints, arXiv:1302.1508.
<https://arxiv.org/abs/1302.1508>
- Capellupo, D. M., Haggard, D., Choux, N., et al. 2017, *ApJ*, 845, 35, doi: [10.3847/1538-4357/aa7da6](https://doi.org/10.3847/1538-4357/aa7da6)
- Dexter, J., Kelly, B., Bower, G. C., et al. 2014, *MNRAS*, 442, 2797, doi: [10.1093/mnras/stu1039](https://doi.org/10.1093/mnras/stu1039)
- Dodds-Eden, K., Porquet, D., Trap, G., et al. 2009, *ApJ*, 698, 676, doi: [10.1088/0004-637X/698/1/676](https://doi.org/10.1088/0004-637X/698/1/676)
- Eckart, A., Schödel, R., Meyer, L., et al. 2006, *A&A*, 455, 1, doi: [10.1051/0004-6361:20064948](https://doi.org/10.1051/0004-6361:20064948)
- Eckart, A., Baganoff, F. K., Morris, M., et al. 2004, *A&A*, 427, 1, doi: [10.1051/0004-6361:20040495](https://doi.org/10.1051/0004-6361:20040495)
- Eckart, A., Schödel, R., García-Marín, M., et al. 2008, *A&A*, 492, 337, doi: [10.1051/0004-6361:200810924](https://doi.org/10.1051/0004-6361:200810924)
- Eckart, A., Baganoff, F. K., Morris, M. R., et al. 2009, *A&A*, 500, 935, doi: [10.1051/0004-6361/200811354](https://doi.org/10.1051/0004-6361/200811354)
- Evans, I. N., Primini, F. A., Glotfelty, K. J., et al. 2010, *ApJS*, 189, 37, doi: [10.1088/0067-0049/189/1/37](https://doi.org/10.1088/0067-0049/189/1/37)
- Fazio, G. G., Hora, J. L., Allen, L. E., et al. 2004, *ApJS*, 154, 10, doi: [10.1086/422843](https://doi.org/10.1086/422843)
- Fazio, G. G., Hora, J. L., Witzel, G., et al. 2018, *ApJ*, 864, 58, doi: [10.3847/1538-4357/aad4a2](https://doi.org/10.3847/1538-4357/aad4a2)
- Fritz, T. K., Gillessen, S., Dodds-Eden, K., et al. 2011, *ApJ*, 737, 73, doi: [10.1088/0004-637X/737/2/73](https://doi.org/10.1088/0004-637X/737/2/73)
- Gravity Collaboration, Abuter, R., Amorim, A., et al. 2019, *A&A*, 625, L10, doi: [10.1051/0004-6361/201935656](https://doi.org/10.1051/0004-6361/201935656)
- Hora, J. L., Witzel, G., Ashby, M. L. N., et al. 2014, *ApJ*, 793, 120, doi: [10.1088/0004-637X/793/2/120](https://doi.org/10.1088/0004-637X/793/2/120)
- Hunter, J. D. 2007, *Computing in Science & Engineering*, 9, 90, doi: [10.1109/MCSE.2007.55](https://doi.org/10.1109/MCSE.2007.55)
- Kluyver, T., Ragan-Kelley, B., Pérez, F., et al. 2016, in *Positioning and Power in Academic Publishing: Players, Agents and Agendas*, ed. F. Loizides & B. Schmidt, IOS Press, 87 – 90
- Marrone, D. P. 2006, PhD thesis, Harvard University
- McKinney, W., et al. 2010, in *Proceedings of the 9th Python in Science Conference*, Vol. 445, Austin, TX, 51–56
- McMullin, J. P., Waters, B., Schiebel, D., Young, W., & Golap, K. 2007, in *Astronomical Society of the Pacific Conference Series*, Vol. 376, *Astronomical Data Analysis Software and Systems XVI*, ed. R. A. Shaw, F. Hill, & D. J. Bell, 127
- Mossoux, E., Grosso, N., Bushouse, H., et al. 2016, *A&A*, 589, A116, doi: [10.1051/0004-6361/201527554](https://doi.org/10.1051/0004-6361/201527554)
- Neilsen, J., Nowak, M. A., Gammie, C., et al. 2013, *ApJ*, 774, 42, doi: [10.1088/0004-637X/774/1/42](https://doi.org/10.1088/0004-637X/774/1/42)
- Pedregosa, F., Varoquaux, G., Gramfort, A., et al. 2011, *Journal of Machine Learning Research*, 12, 2825
- Peterson, B. M., Wanders, I., Horne, K., et al. 1998, *PASP*, 110, 660, doi: [10.1086/316177](https://doi.org/10.1086/316177)
- Scargle, J. D. 1998, *ApJ*, 504, 405, doi: [10.1086/306064](https://doi.org/10.1086/306064)
- Scargle, J. D., Norris, J. P., Jackson, B., & Chiang, J. 2013, *ApJ*, 764, 167, doi: [10.1088/0004-637X/764/2/167](https://doi.org/10.1088/0004-637X/764/2/167)
- Sun, M., Grier, C. J., & Peterson, B. M. 2018, *PyCCF: Python Cross Correlation Function for reverberation mapping studies*. <http://ascl.net/1805.032>
- van der Laan, H. 1966, *Nature*, 211, 1131, doi: [10.1038/2111131a0](https://doi.org/10.1038/2111131a0)
- Virtanen, P., Gommers, R., Oliphant, T. E., et al. 2020, *Nature Methods*, 17, 261, doi: <https://doi.org/10.1038/s41592-019-0686-2>
- Werner, M. W., Roellig, T. L., Low, F. J., et al. 2004, *ApJS*, 154, 1, doi: [10.1086/422992](https://doi.org/10.1086/422992)
- Williams, P. K. G., Clavel, M., Newton, E., & Ryzhkov, D. 2017, *pwkit: Astronomical utilities in Python*. <http://ascl.net/1704.001>
- Witzel, G., Martinez, G., Hora, J., et al. 2018, *ApJ*, 863, 15, doi: [10.3847/1538-4357/aace62](https://doi.org/10.3847/1538-4357/aace62)
- Yusef-Zadeh, F., Roberts, D., Wardle, M., Heinke, C. O., & Bower, G. C. 2006, *ApJ*, 650, 189, doi: [10.1086/506375](https://doi.org/10.1086/506375)
- Yusef-Zadeh, F., Wardle, M., Heinke, C., et al. 2008, *ApJ*, 682, 361, doi: [10.1086/588803](https://doi.org/10.1086/588803)
- Zylka, R., Mezger, P. G., & Lesch, H. 1992, *A&A*, 261, 119
- Zylka, R., Mezger, P. G., Ward-Thompson, D., Duschl, W. J., & Lesch, H. 1995, *A&A*, 297, 83. <https://arxiv.org/abs/astro-ph/9410086>